JACS
JOURNAL OF THE AMERICAN CHEMICAL SOCIETY
pubs.acs.org/JACS
Communication

# Benchmarking the Reactivity of Caged Iron(IV)-Oxo Sites within Metal−Organic Frameworks

Jonas Börgel, Yuan Cao, Ran Gao, Daniel C. Y. Leong, Rachel Narehood Austin,* John T. Groves,* and Jeffrey R. Long*

Cite This: J. Am. Chem. Soc. 2025, 147, 21325−21330
Read Online
ACCESS | Metrics & More | Article Recommendations | Supporting Information

**ABSTRACT:** Three recently reported iron-containing metal−organic frameworks, $FeZn_4(prv)_4(btdd)_3$ (Fe-**1**), $Fe_{1.8}Zn_{3.2}(prv)_4(btdd)_3$ ($Fe_{1.8}$-**1**), and $FeZn_4(moba)_4(btdd)_3$ (Fe-**2**) (Hprv = pyruvic acid, Hmoba = 3,3-dimethyl-2-oxobutanoic acid, and $H_2$btdd = bis(1*H*-1,2,3-triazolo[4,5-*b*],[4′,5′-*i*])dibenzo[1,4]dioxin), that react with $O_2$ at low temperatures to generate high-spin ($S$ = 2) ferryl species provide an unprecedented opportunity to explore the effects of spin state and site-isolation on hydrocarbon oxidation reaction mechanisms. These reagents oxidize the radical clock substrate norcarane, yielding radical lifetimes in the low nanosecond regime, consistent with a diffusion-limited rebound mechanism. Rebound products derived from ligands on the iron centers inside the framework are detected and recapitulate chemistry seen in the structurally related $\alpha$-ketoglutarate-dependent dioxygenases such as TauD, which also generate high-spin ($S$ = 2) ferryl intermediates. Framework models indicate that productive reactions occur when norcarane approaches the ferryl species from the larger of the two pores of the MFU-4*l*-type framework.



Isolating reaction centers is a powerful strategy for limiting unwanted side reactions and increasing selectivity.[1−4] Early forays in biomimetic chemistry created structures to geometrically constrain reaction partners and steer reactions toward desired products.[5−7] More recently, research has flourished in areas of molecular containers, metal−organic frameworks (MOFs), and mesoporous materials, which offer synthetic approaches to tailor solvent and solute access to reactive sites. Porous materials have successfully stabilized reactive intermediates not seen in noncaged systems.[8−11]

Metal−organic framework materials that generate high-spin ($S$ = 2) $Fe^{IV}$=O sites provide an informative platform for exploring the features that control C−H oxygenation reactions (Figure 1A).[12] The iron-containing frameworks $FeZn_4(prv)_4(btdd)_3$ (Fe-**1**), $Fe_{1.8}Zn_{3.2}(prv)_4(btdd)_3$ ($Fe_{1.8}$-**1**), and $FeZn_4(moba)_4(btdd)_3$ (Fe-**2**), where Hprv = pyruvic acid, Hmoba = 3,3-dimethyl-2-oxobutanoic acid, and $H_2$btdd = bis(1*H*-1,2,3-triazolo[4,5-*b*],[4′,5′-*i*])dibenzo-[1,4]dioxin), react with $O_2$ at low temperatures to decarboxylate the $\alpha$-ketoacid ligand and generate an $Fe^{IV}$=O intermediate in a manner reminiscent of $\alpha$-ketoglutarate-dependent dioxygenases such as TauD.[13−16] The $Fe^{IV}$=O sites within these materials, hereafter referred to as ferrylMOFs, were shown to hydroxylate simple alkanes, presumably via an H atom transfer (HAT) and radical rebound mechanism (Figure 1B). Herein, we examine the C−H oxygenation chemistry of all three MOFs to probe whether the confined reaction space within the pores recapitulates the restricted behavior detected in metalloenzyme systems, where the fate of enzyme-generated substrate radicals is limited to the production of only a few products.[17−28] To that end, the radical clock probe, bicyclo[4.1.0]heptane (norcarane) was used as a substrate for the three ferrylMOFs.[29,30]

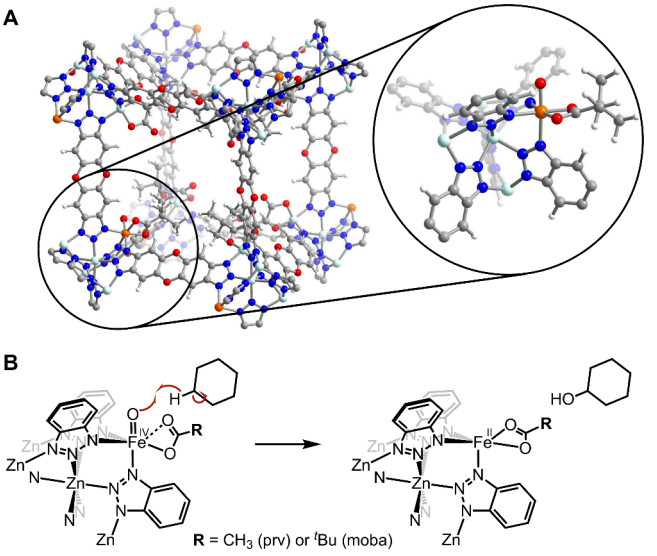


**Figure 1.** (**A**) Structural illustration of one cubic pore of $FeZn_4(moba)_4(btdd)_3$ after reaction with $O_2$ and $\alpha$-ketoacid ligand decarboxylation. The inset shows the truncated structure around the cluster node containing the $Fe^{IV}$=O site. Light blue, orange, red, blue, gray, and white spheres represent Zn, Fe, O, N, C, and H atoms, respectively. (**B**) Schematic representation of HAT from cyclohexane by an $Fe^{IV}$=O site followed by radical rebound to form cyclohexanol.

**Received:** April 2, 2025
**Revised:** June 5, 2025
**Accepted:** June 6, 2025
**Published:** June 11, 2025





https://doi.org/10.1021/jacs.5c05557
J. Am. Chem. Soc. 2025, 147, 21325−21330

The results from the three frameworks were broadly similar. Each ferrylMOF reacted with norcarane to generate a range of oxidized products indicative of radical rebound (Figures 2, S1, and S2).[31] Table S1 provides the amounts of all norcarane-derived products, normalized to experimentally determined response factors where available or to estimated response factors based on calculated effective carbon numbers (ECN)[32] where experimentally determined response factors were not available, from the nine stoichiometric reactions performed.

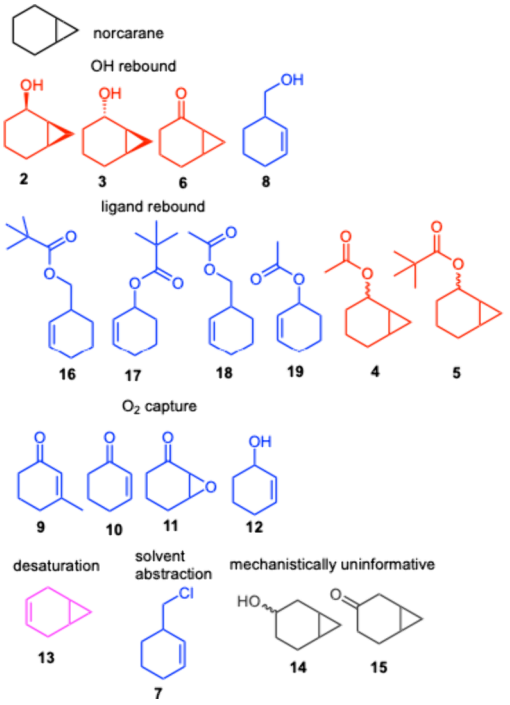


**Figure 2.** Overview of all norcarane-derived products (blue = rearranged; red = unrearranged; pink = desaturated, gray = mechanistically uninformative) (see the Supporting Information for details).

Figures 3 and S4 show representative chromatograms from the oxidation of norcarane by Fe-**1** and $Fe_{1.8}$-**1** respectively. The measured substrate radical lifetimes are all in the low *nanosecond* regime (Table 1). A comparison reaction with $FeZn_4Cl_4(btdd)_3$ (Fe-**3**)—which has no $\alpha$-ketoacid ligand to enable the generation of $Fe^{IV}$=O sites—showed only minute amounts of some products. Given the low yield of such products, including or not including the compounds found in the comparison reactions in the analysis of the reactions carried out by the ferrylMOFs did not impact the conclusions.

**Table 1. Summary of the Radical Lifetimes Determined for Reactions of Norcarane with the Three ferrylMOFs from Two Separate Reactions in $CD_2Cl_2$ and $CD_3CN$ (The Color Separates the Reactions by ferrylMOF)**

| Fe-MOF | Probe | Solvent | Lifetime (ns) |
|---|---|---|---|
| **Fe-3** | Norcarane | $CD_2Cl_2$ $CD_3CN$ | comparison |
| **Fe-1** | Norcarane | $CD_2Cl_2$ | 3.6, 11.7 |
| **Fe-1** | Norcarane | $CD_3CN$ | 14.1 |
| **$Fe_{1.8}$-1** | Norcarane | $CD_2Cl_2$ | 3.4, 10.2 |
| **$Fe_{1.8}$-1** | Norcarane | $CD_3CN$ | 12.1 |
| **Fe-2** | Norcarane | $CD_2Cl_2$ | 4.8, 4.9 |
| **Fe-2** | Norcarane | $CD_3CN$ | 12.3 |

Significantly, appreciable amounts of products consistent with $\alpha$-ketoacid-derived ligand rebound to the norcaranyl radical were detected. Both the ring-opened product cyclohex-2-en-1-yl-methylpivalate (**16**) and the ring-closed product bicyclo[4.1.0]heptan-2-ylpivalate (**5**) were detected in reactions with Fe-**2**, comprising ~19% of all norcarane-derived products. Relatively less cyclohex-2-en-1-yl-methyl acetate

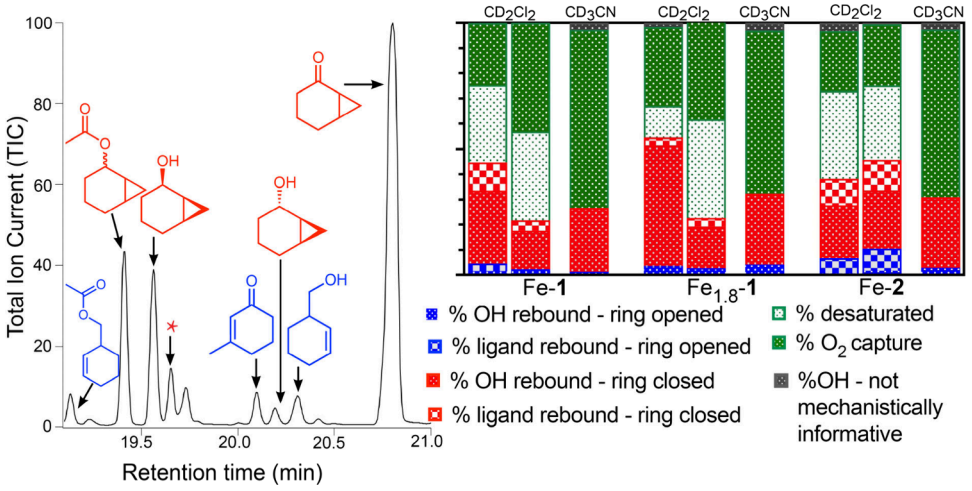


**Figure 3.** Illustrative chromatogram of a norcarane oxidation reaction with Fe-**1** coupled to a product summary of the results of all norcarane oxidation reactions with the ferrylMOFs in two solvents, $CD_2Cl_2$ and $CD_3CN$. Each column represents the results from a separate reaction. The last reaction in each set was performed in $CD_3CN$. Products of $O_2$ capture followed by ligand rebound were included in the $O_2$ capture chemotype. The other isomer of bicyclo[4.1.0]heptan-2-yl acetate (cpd **4**) is indicated with a red asterisk.



https://doi.org/10.1021/jacs.5c05557
J. Am. Chem. Soc. 2025, 147, 21325−21330

(**18**) and bicyclo[4.1.0]heptan-2-ylacetate (**4**) were detected in the reactions with Fe-**1** or $Fe_{1.8}$-**1**.

We examined the reactions of the ferrylMOFs in two different solvents, $CD_2Cl_2$ and $CD_3CN$, noting minor differences. Both desaturation and ligand rebound products were more prevalent in $CD_2Cl_2$ (Figures 2, 3, and 4; Table S1).[33] Very small amounts of ligand rebound products were detected in reactions performed in $CD_3CN$.

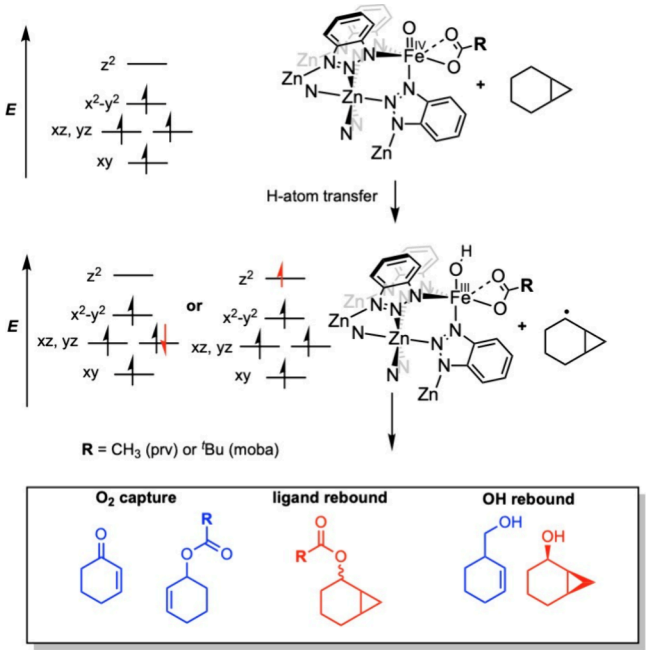


**Figure 4.** Overview of norcarane oxidation products generated with Fe-**2** and $O_2$. The electron transferred during HAT can reside in either the $d_{z^2}$ orbital in the $\sigma$-pathway, which maximizes spin polarization, or the $d_{xz}$, $d_{yz}$ orbital pair in the $\pi$-pathway.

Some products consistent with migration of the substrate radical from the site of generation and capture by $O_2$ were also detected (Figure 2). Consistent with the increased solubility of $O_2$ in acetonitrile,[34,35] more $O_2$-capture products were detected in reactions run in $CD_3CN$. Cyclohexenone (**10**), detected in reactions with norcarane, can form from $O_2$ capture by the 3-cyclohexenylmethyl radical followed by elimination of formaldehyde (as demonstrated in Figure S14 from the tetrabutylammonium decatungstate (TBADT) photocatalyzed oxidation of norcarane in $O_2$).[36]

High-spin ($S$ = 2) species have been predicted to be better oxidants for HAT reactions,[37,38] although recently $S$ = 1 model complexes have been developed that have HAT rates as fast or faster than $S$ = 2 model systems and can catalyze reactions similar to their $S$ = 2 counterparts.[39−42] Our results do not allow us to disentangle site-isolation and iron spin state factors unambiguously. However, comparing our results with results reported for $[(TQA)ClFe^{IV}O]^+$ (TQA = tris(quinolyl-2-methyl)amine) in solution is informative.[38] This molecular $S$ = 2 species, which is structurally similar to the reactive ferrylMOF species herein, mediates the oxidation and halogenation of cyclohexane.[38] The majority of products from the reaction of $[(TQA)ClFe^{IV}O]^+$ with cyclohexane were chlorinated (78%); cyclohexanol comprised only 15% of the products. Addition of $O_2$ suppressed the formation of halogenated products when using $[(TQA)ClFe^{IV}O]^+$, indicating that radical escape from the solvent cage dominated the reactivity of this species. In contrast, for all three ferrylMOFs, a substantial fraction of the radicals generated from HAT rebound with the $Fe^{III}$−OH species or the associated carboxylate ligand before the radical clocks can rearrange, pointing to the important role that confinement inside the MOF is playing in the chemistry.[43]

The 4−12 ns radical lifetime measured for the ferrylMOF reactions with norcarane are an order of magnitude longer than those measured for the nonheme diiron enzymes toluene monooxygenase (T4MO) and soluble methane monooxygenase (sMMO) and 2 orders of magnitude longer than those measured for metalloporphyrins and cytochrome P450 (CYP) enzymes.[20,23,27,44,45] However, the low nanosecond lifetimes are considerably shorter than those measured for freely diffusing radicals generated by photochemical bond cleavage in solution (see Figure S14 for the GC trace of products from decatungstate oxidation of norcarane).[27,45,23] One reason for the difference in radical lifetimes may be that the catalytically active intermediates in T4MO, sMMO, and CYP are formally one oxidation state higher than that of the reactive intermediate in the ferrylMOFs. The rebound oxidant in the ferrylMOF reactions is an $Fe^{III}$−OH species, typical of $\alpha$-ketoglutarate-dependent enzymes, whereas $Fe^{IV}$ intermediates capture the substrate radical during turnover with T4MO, sMMO, and CYP (Figure 4).

Figure 5 shows a model of two adjacent pores of $FeZn_4(moba)_4(btdd)_3$ (Fe-**2**), a larger A-pore (with an internal diameter of ⌀ ≈ 19 Å) and a smaller B-pore (⌀ ≈ 8 Å).[41] The

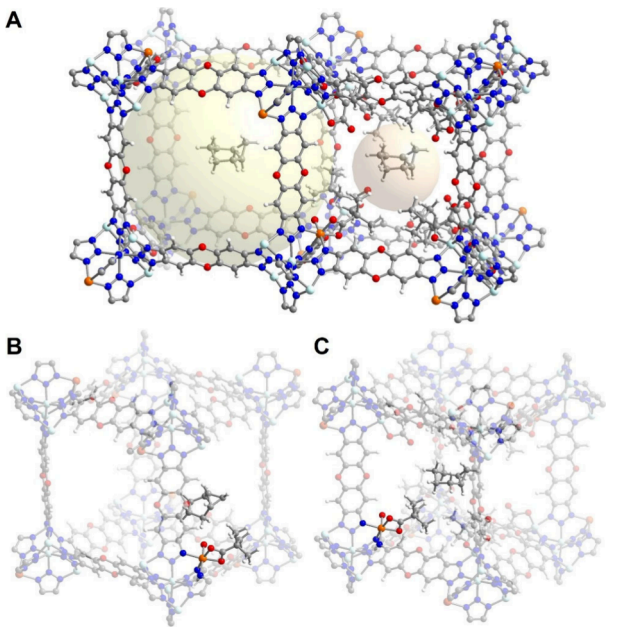


**Figure 5.** (**A**) Illustration of the adjacent large (A-pore) and small (B-pore) of $O_2$-exposed Fe-**2**, with a norcarane molecule placed in the center of each pore. The transparent yellow and orange spheres indicate the accessible pore volumes. (**B**) Approach of norcarane to the $Fe^{IV}$=O species from the A-pore; $Fe^{IV}$=O site can be accessed for HAT. (**C**) Approach of norcarane to the $Fe^{IV}$=O species from the B-pore; $Fe^{IV}$=O site cannot be accessed for HAT. Only norcarane and the $Fe^{IV}$=O site are accentuated for clarity. Light blue, orange, red, blue, gray, and white spheres represent Zn, Fe, O, N, C, and H atoms, respectively. The moba and pivalate ligands not pointed into the depicted pores have been omitted for clarity.



https://doi.org/10.1021/jacs.5c05557
J. Am. Chem. Soc. 2025, 147, 21325−21330

model of the framework after decarboxylation was derived from structures obtained by single-crystal X-ray analysis.[12] The carboxylate ligands coordinated to the peripheral metal centers of each node point only into the B-pores, leading to a smaller accessible volume for guest molecules. Our model suggests that norcarane molecules can diffuse through both the A- and B-pores of the framework despite the smaller volume of the latter (Figures 5A and S20). However, the relevant orbitals for HAT of the reactive high-spin $Fe^{IV}$=O site can only be approached by norcarane from the larger A-pore and not from the smaller B-pore (Figures 5B and 5C), because the bulky *t*-Bu group of the pivalate ligand prevents the optimal approach of norcarane for HAT. Although the smaller B-pores in the ferrylMOFs (Fe-**1** and Fe-**2**) have significant differences in size depending on the $\alpha$-ketoacid ligand ($\varnothing \approx 8$ Å (moba) to $\varnothing \approx 10$ Å (prv)), the radical lifetimes are relatively independent of the size of the $\alpha$-ketocarboxylate ligand, which suggests a similar substrate approach from the larger A-pore in both Fe-**1** and Fe-**2**.

The notably large *intermolecular* hydrogen isotope effect of ~ 30 observed for the oxidation of cyclohexane (H/D) by Fe-**1**[12] requires rapid exchange of the substrate molecules in the pores positioned adjacent to the $Fe^{IV}$=O species for HAT. From the iron-exchange stoichiometry, we expect between 2.0 and 3.6 iron centers arranged at the vertices of a cube and positioned at the intersection of the large and small framework pores. Diffusion rates in solution enable molecules to move ~ 1 Å per ns, while diffusion within a porous framework would be expected to be somewhat slower.[3,46] Thus, from geometric arguments alone, radical movement in this reaction scenario would be limited. Accordingly, the 4−12 ns radical lifetimes observed for the diffusing and rearranging radical clock substrates are commensurate with the size of the (larger) reaction cavity. It appears from the data that the ferrylMOFs diminish fast radical motion away from the reaction center relative to a radical generated by an $S = 2$ mononuclear $Fe^{IV}$=O species in solution.

Members of the nonheme mononuclear $Fe^{II}$/$\alpha$-ketoglutarate-dependent halogenases are notable for their ability to redirect the canonical oxygen-rebound mechanism to iron-coordinated halogen atoms, affording halogenated products.[47,14,48] The presence of two reaction channels from the high-spin $Fe^{IV}$=O intermediate in these enzymes has been invoked in enabling the ligand rebound chemistry (Figure 4).[49,50] The position of the substrate relative to the metal−oxygen bond may also be important, and is influenced by geometric flexibility at the active site.[51,52] The reaction with norcarane generates products that arise from rebound of an iron-coordinated carboxylate ligand, for which our model suggests that at least one carboxylate oxygen atom would be accessible for rebound via alkyl radical approach from the large A-pore (Figure S21). Such ligand rebound reactions are suppressed in acetonitrile. It is likely that acetonitrile coordinates the iron center, in lieu of $\kappa^2$-coordination of the carboxylate, as is known for $[(TQA)(MeCN)Fe^{IV}O]^+$ and similar ferryl species.[38,53] This change in coordination environment could render carboxylate rebound statistically less likely because the now $\kappa^1$-bound carboxylate may not be geometrically available for C−O bond formation through radical rebound.[53] Alternatively, a change in coordination could alter the oxidation potential of the ferric intermediate and disfavor ligand rebound. Ligand and/or solvent rebound products have been observed before in nonheme Mn catalysts as well.[54,55]

In conclusion, the opportunity provided by this unique set of metal−organic frameworks to study a well-characterized high-spin $Fe^{IV}$=O species provides important information about the factors that govern the reactivity of metal-oxo complexes and the dynamics of substrate radical intermediates within MOF cavities. These results show that the site-isolated high-spin $S = 2$ $Fe^{IV}$=O intermediates generate norcaranyl radicals with low nanosecond lifetimes, which is consistent with radical diffusion within the diameter of the larger A pores. This work contributes nuanced experimental data to ongoing efforts to resolve the role of geometric and electronic factors in controlling HAT and functionalization.

## ■ ASSOCIATED CONTENT

### Supporting Information

The Supporting Information is available free of charge at https://pubs.acs.org/doi/10.1021/jacs.5c05557.

Additional experimental information, product identification information, additional images of framework and substrate interactions (PDF)

## ■ AUTHOR INFORMATION


### Corresponding Authors

**Rachel Narehood Austin** − *Department of Chemistry, Barnard College, New York, New York 10027, United States;* orcid.org/0000-0001-9233-4443; Email: rna2113@columbia.edu

**John T. Groves** − *Department of Chemistry, Princeton University, Princeton, New Jersey 08544, United States;* orcid.org/0000-0002-9944-5899; Email: jtgroves@princeton.edu

**Jeffrey R. Long** − *Department of Chemistry, University of California, Berkeley, California 94720, United States; Materials Sciences Division, Lawrence Berkeley National Laboratory, Berkeley, California 94720, United States; Department of Chemical and Biomolecular Engineering and Department of Materials Science and Engineering, University of California, Berkeley, California 94720, United States;* orcid.org/0000-0002-5324-1321; Email: jrlong@berkeley.edu

### Authors

**Jonas Börgel** − *Department of Chemistry, University of California, Berkeley, California 94720, United States; Materials Sciences Division, Lawrence Berkeley National Laboratory, Berkeley, California 94720, United States;* Present Address: Department of Chemistry, New York University, New York, New York 10003, United States; orcid.org/0000-0001-5301-8579

**Yuan Cao** − *Department of Chemistry, Princeton University, Princeton, New Jersey 08544, United States;* Present Address: Department of Chemistry, Columbia University, New York, New York 10027, United States

**Ran Gao** − *Department of Chemistry, Princeton University, Princeton, New Jersey 08544, United States*

**Daniel C. Y. Leong** − *Department of Chemistry, University of California, Berkeley, California 94720, United States*

Complete contact information is available at: https://pubs.acs.org/10.1021/jacs.5c05557

### Funding

NIH RO1 GM130989 to R.N.A., NSF CHE-2246289 to J.T.G., and DoE DE-SC0019992 to J.R.L.

### Notes

The authors declare no competing financial interest.

## ■ ACKNOWLEDGMENTS

Research reported in this publication was supported by the National Institute of General Medical Sciences of the National Institutes of Health under award number R01 GM130989 to R.N.A. by the National Science Foundation under award CHE-2246289 to J.T.G. and by the U.S. Department of Energy, Office of Basic Energy Sciences (BES), Separation Science in the Chemical Sciences, Geosciences, and Biosciences Division, under award number DE-SC0019992 to J.R.L. We thank Yuto Yabuuchi for assistance with calculating accessible pore volumes and for helpful discussions.

## ■ ABBREVIATIONS

Hprv, pyruvic acid; Hmoba, 3,3-dimethyl-2-oxobutanoic acid; $H_2$btdd, bis(1*H*-1,2,3-triazolo[4,5-*b*],[4′,5′-*i*])dibenzo[1,4]-dioxin; MOF, metal−organic framework; T4MO, toluene monooxygenase; sMMO, soluble methane monooxygenase; CYP, cytochrome P450; HAT, hydrogen atom transfer

## ■ REFERENCES

(1) Petroselli, M.; Angamuthu, V.; Rahman, F.-U.; Zhao, X.; Yu, Y.; Rebek, J., Jr Radical Reactions in Cavitands Unveil the Effects of Affinity on Dynamic Supramolecular Systems. *J. Am. Chem. Soc.* **2020**, *142* (5), 2396−2403.

(2) Yu, Y.; Yang, J.-M.; Rebek, J. Molecules in Confined Spaces: Reactivities and Possibilities in Cavitands. *Chem.* **2020**, *6* (6), 1265−1274.

(3) Gao, W.-Y.; Cardenal, A. D.; Wang, C.-H.; Powers, D. C. In Operando Analysis of Diffusion in Porous Metal-Organic Framework Catalysts. *Chem.—Eur. J.* **2019**, *25*, 3465−3476.

(4) Snyder, B. E. R.; Bols, M. L.; Rhoda, H. M.; Plessers, D.; Schoonheydt, R. A.; Sels, B. F.; Solomon, E. I. Cage effects control the mechanism of methane hydroxylation in zeolites. *Science* **2021**, *373* (6552), 327−331.

(5) Tawfik, D. S. Accuracy-rate tradeoffs: how do enzymes meet demands of selectivity and catalytic efficiency? *Curr. Opin. Chem. Biol.* **2014**, *21*, 73−80.

(6) Breslow, R. Centenary Lecture. Biomimetic chemistry. *Chem. Soc. Rev.* **1972**, *1* (4), 553−580.

(7) Breslow, R. Biomimetic control of chemical selectivity. *Acc. Chem. Res.* **1980**, *13* (6), 170−177.

(8) Gera, R.; De, P.; Singh, K. K.; Jannuzzi, S. A. V.; Mohanty, A.; Velasco, L.; Kulbir; Kumar, P.; Marco, J. F.; Nagarajan, K.; Pecharromán, C.; Rodríguez-Pascual, P. M.; DeBeer, S.; Moonshiram, D.; Gupta, S. S.; Dasgupta, J. Trapping an Elusive Fe(IV)-Superoxo Intermediate Inside a Self-Assembled Nanocage in Water at Room Temperature. *J. Am. Chem. Soc.* **2024**, *146* (31), 21729−21741.

(9) Herron, N. The Selective Partial Oxidation of Alkanes using Zeolite Based Catalysts. Phthalocyanine (PC) "Ship-in-Bottle" Species. *J. Coord. Chem.* **1988**, *19* (1−3), 25−38.

(10) Parton, R. F.; Vankelecom, I. F. J.; Casselman, M. J. A.; Bezoukhanova, C. P.; Uytterhoeven, J. B.; Jacobs, P. A. An efficient mimic of cytochrome P-450 from a zeolite-encaged iron complex in a polymer membrane. *Nature* **1994**, *370* (6490), 541−544.

(11) Saghian, M.; Dehghanpour, S.; Sharbatdaran, M. "Ship in a bottle" Porph@MOMs as highly efficient catalysts for selective controllable oxidation and insights into different mechanisms in heterogeneous and homogeneous environments. *New J. Chem.* **2018**, *42* (15), 12872−12881.

(12) Hou, K.; Börgel, J.; Jiang, H. Z. H.; SantaLucia, D. J.; Kwon, H.; Zhuang, H.; Chakarawet, K.; Rohde, R. C.; Taylor, J. W.; Dun, C.; Paley, M. V.; Turkiewicz, A. B.; Park, J. G.; Mao, H.; Zhu, Z.; Alp, E. E.; Zhao, J.; Hu, M. Y.; Lavina, B.; Peredkov, S.; Lv, X.; Oktawiec, J.; Meihaus, K. R.; Pantazis, D. A.; Vandone, M.; Colombo, V.; Bill, E.; Urban, J. J.; Britt, R. D.; Grandjean, F.; Long, G. J.; DeBeer, S.; Neese, F.; Reimer, J. A.; Long, J. R. Reactive high-spin iron(IV)-oxo sites through dioxygen activation in a metal-organic framework. *Science* **2023**, *382* (6670), 547−553.

(13) Kovaleva, E. G.; Lipscomb, J. D. Versatility of biological non-heme Fe(II) centers in oxygen activation reactions. *Nat. Chem. Biol.* **2008**, *4* (3), 186−193.

(14) Krebs, C.; Galonic Fujimori, D.; Walsh, C. T.; Bollinger, J. M. Non-heme Fe(IV)-oxo intermediates. *Acc. Chem. Res.* **2007**, *40* (7), 484−492.

(15) Price, J. C.; Barr, E. W.; Tirupati, B.; Bollinger, J. M., Jr.; Krebs, C. The first direct characterization of a high-valent iron intermediate in the reaction of an alpha-ketoglutarate-dependent dioxygenase: a high-spin FeIV complex in taurine/alpha-ketoglutarate dioxygenase (TauD) from Escherichia coli. *Biochemistry* **2003**, *42* (24), 7497−7508.

(16) Sinnecker, S.; Svensen, N.; Barr, E. W.; Ye, S.; Bollinger, J. M., Jr.; Neese, F.; Krebs, C. Spectroscopic and computational evaluation of the structure of the high-spin Fe(IV)-oxo intermediates in taurine: alpha-ketoglutarate dioxygenase from Escherichia coli and its His99Ala ligand variant. *J. Am. Chem. Soc.* **2007**, *129* (19), 6168−6179.

(17) Austin, R. N.; Bertrand, E. M.; Groves, J. T.; Vetriani, C.; Keddis, R. Identity and mechanisms of alkane-oxidizing metalloenzymes from deep-sea hydrothermal vents. *Front. Microbiol.* **2013**, *4*, 109.

(18) Austin, R. N.; Buzzi, K.; Kim, E.; Zylstra, G.; Groves, J. T. Xylene Monooxygenase, a membrane-spanning non-heme diiron enzyme that hydroxylates hydrocarbons via a substrate radical intermediate. *J. Biol. Inorg. Chem.* **2003**, *8*, 733−740.

(19) Austin, R. N.; Chang, H.-K.; Zylstra, G.; Groves, J. T. The Non-Heme Diiron Alkane Monooxygenase of Pseudomonas oleovorans (AlkB) Hydroxylates via a Substrate Radical Intermediate. *J. Am. Chem. Soc.* **2000**, *122*, 11747−11748.

(20) Austin, R. N.; Deng, D.; Jiang, Y.; Luddy, K.; van Beilen, J. B.; Ortiz de Montellano, P. R.; Groves, J. T. The diagnostic substrate bicyclohexane reveals a radical mechanism for bacterial Cytochrome P450 in whole cells. *Angew. Chem., Int. Ed.* **2006**, *45*, 8192−8194.

(21) Austin, R. N.; Luddy, K.; Erickson, K.; Pender-Cudlip, M.; Bertrand, E. M.; Deng, D.; Buzdygon, R. S.; van Beilen, J. B.; Groves, J. T. Cage escape competes with geminate recombination during alkane hydroxylation by the diiron oxygenase AlkB. *Angew. Chem., Int. Ed.* **2008**, *47* (28), 5232−5234.

(22) Bertrand, E. M.; Sakai, R.; Rozhkova-Novosad, E. A.; Moe, L. A.; Fox, B. G.; Groves, J. T.; Austin, R. N. Reaction mechanisms of non-heme diiron hydroxylases characterized in whole cell. *J. Inorg. Biochem.* **2005**, *99*, 1998−2006.

(23) Brazeau, B. J.; Austin, R. N.; Tarr, C.; Groves, J. T.; Lipscomb, J. D. Intermediate Q from soluble Methane Monooxygenase (sMMO) hydroxylates the mechanistic substrate probe norcarane: Evidence for a Stepwise Reaction. *J. Am. Chem. Soc.* **2001**, *123*, 11831−11837.

(24) Chakrabarty, S.; Austin, R. N.; Deng, D.; Groves, J. T.; Lipscomb, J. D. Radical Intermediates in Monooxygenase Reactions of Rieske Dioxygenase. *J. Am. Chem. Soc.* **2007**, *129*, 3514−3515.

(25) Cooper, H. L. R.; Mishra, G.; Huang, X.; Pender-Cudlip, M.; Austin, R. N.; Shanklin, J.; Groves, J. T. Parallel and Competitive Pathways for Substrate Desaturation, Hydroxylation, and Radical Rearrangement by the Non-heme Diiron Hydroxylase AlkB. *J. Am. Chem. Soc.* **2012**, *134*, 20365−20375.

(26) Hsieh, C. H.; Huang, X.; Amaya, J. A.; Rutland, C. D.; Keys, C. L.; Groves, J. T.; Austin, R. N.; Makris, T. M. The Enigmatic P450 Decarboxylase OleT Is Capable of, but Evolved To Frustrate, Oxygen Rebound Chemistry. *Biochemistry* **2017**, *56* (26), 3347−3357.

(27) Moe, L. A.; Hu, Z.; Deng, D.; Austin, R. N.; Groves, J. T.; Fox, B. G. Remarkable Aliphatic Hydroxylation by Diiron Enzyme Toluene 4-Monooxygenase in Reactions with Radical/Cation Diagnostic Probes Norcarane, 1,1-Dimethylcyclopropane, and 1,1-Diethylcyclopropane. *Biochemistry* **2004**, *43* (50), 15688−15701.
(28) Williams, S. C.; Forsberg, A. P.; Lee, J.; Vizcarra, C. L.; Lopatkin, A. J.; Austin, R. N. Investigation of the prevalence and catalytic activity of rubredoxin-fused alkane monooxygenases (AlkBs). *J. Inorg. Biochem.* **2021**, *219*, 111409.
(29) Bowry, V. W.; Lusztyk, J.; Ingold, K. U. Calibration of a new horology of fast radical clocks. Ring-opening rates for ring-and.alpha.-alkyl-substituted cyclopropylcarbinyl radicals and for the bicyclo[2.1.0]pent-2-yl radical. *J. Am. Chem. Soc.* **1991**, *113* (15), 5687−5698.
(30) Auclair, K.; Hu, Z.; Little, D. M.; Ortiz de Montellano, P. R.; Groves, J. T. Revisiting the mechanism of P450 enzymes with the radical clocks norcarane and spiro[2,5]octane. *J. Am. Chem. Soc.* **2002**, *124*, 6020−6027.
(31) Huang, X. Y.; Groves, J. T. Beyond ferryl-mediated hydroxylation: 40 years of the rebound mechanism and C-H activation. *J. Biol. Inorg. Chem.* **2017**, *22*, 185−207.
(32) Szulejko, J. E.; Kim, K.-H. Re-evaluation of effective carbon number (ECN) approach to predict response factors of 'compounds lacking authentic standards or surrogates' (CLASS) by thermal desorption analysis with GC-MS. *Anal. Chim. Acta* **2014**, *851*, 14−22.
(33) Dantignana, V.; Pérez-Segura, M. C.; Besalú-Sala, P.; Delgado-Pinar, E.; Martínez-Camarena, Á.; Serrano-Plana, J.; Álvarez-Núñez, A.; Castillo, C. E.; García-España, E.; Luis, J. M.; Basallote, M. G.; Costas, M.; Company, A. Characterization of a Ferryl Flip in Electronically Tuned Nonheme Complexes. Consequences in Hydrogen Atom Transfer Reactivity. *Angew. Chem., Int. Ed.* **2023**, *62* (2), No. e202211361.
(34) Quaranta, M.; Murkovic, M.; Klimant, I. A new method to measure oxygen solubility in organic solvents through optical oxygen sensing. *Analyst* **2013**, *138* (21), 6243−6245.
(35) Sato, T.; Hamada, Y.; Sumikawa, M.; Araki, S.; Yamamoto, H. Solubility of Oxygen in Organic Solvents and Calculation of the Hansen Solubility Parameters of Oxygen. *Ind. Eng. Chem. Res.* **2014**, *53* (49), 19331−19337.
(36) Büker, J.; Peng, B. Mechanistic insights into liquid-phase autoxidation of cyclohexene in acetonitrile. *Mol. Catal.* **2022**, *525*, 112367.
(37) Gordon, J. B.; Albert, T.; Dey, A.; Sabuncu, S.; Siegler, M. A.; Bill, E.; Moënne-Loccoz, P.; Goldberg, D. P. A Reactive, Photogenerated High-Spin (S = 2) Fe(IV)(O) Complex via $O_2$ Activation. *J. Am. Chem. Soc.* **2021**, *143* (51), 21637−21647.
(38) Puri, M.; Biswas, A. N.; Fan, R.; Guo, Y.; Que, L. J. Modeling Non-Heme Iron Halogenases: High-Spin Oxoiron(IV)-Halide Complexes that Halogenate C-H Bonds. *J. Am. Chem. Soc.* **2016**, *138*, 2484−2487.
(39) Das, A.; Pal, N.; Xiong, J.; Young, V. G., Jr.; Guo, Y.; Swart, M.; Que, L. Jr. 10-Fold Increase in Hydrogen Atom Transfer Reactivity for a Series of S = 1 FeIV═O Complexes Over the S = 2 $[(TQA)FeIV═O]^{2+}$ Complex via Entropic Lowering of Reaction Barriers by Secondary Sphere Cycloalkyl Substitution. *J. Am. Chem. Soc.* **2025**, *147* (1), 292−304.
(40) Bleher, K.; Comba, P.; Faltermeier, D.; Gupta, A.; Kerscher, M.; Krieg, S.; Martin, B.; Velmurugan, G.; Yang, S. Non-Heme-Iron-Mediated Selective Halogenation of Unactivated Carbon-Hydrogen Bonds. *Chem.—Eur. J.* **2022**, *28* (4), No. e202103452.
(41) Janardanan, D.; Wang, Y.; Schyman, P.; Que, L., Jr.; Shaik, S. The fundamental role of exchange-enhanced reactivity in C-H activation by S = 2 oxo iron(IV) complexes. *Angew. Chem., Int. Ed. Engl.* **2010**, *49* (19), 3342−3345.
(42) Cho, K.-B.; Hirao, H.; Shaik, S.; Nam, W. To rebound or dissociate? This is the mechanistic question in C-H hydroxylation by heme and nonheme metal-oxo complexes. *Chem. Soc. Rev.* **2016**, *45*, 1197−1210.
(43) Cardenal, A. D.; Jeong Park, H.; Chalker, C. J.; Ortiz, K. G.; Powers, D. C. cis-Decalin oxidation as a stereochemical probe of in-MOF versus on-MOF catalysis. *Chem. Commun.* **2017**, *53* (53), 7377−7380.
(44) Naing, S.-H.; Parvez, S.; Pender-Cudlip, M.; Groves, J. T.; Austin, R. N. Substrate specificity and reaction mechanism of purified alkane hydroxylase (AlkB) from the hydrocarbonoclastus bacterium Alcanivorax borkumensis. *J. Inorg. Biochem.* **2013**, *121*, 46−52.
(45) Rozhkova-Novosad, E. A.; Chae, J.-C.; Zylstra, G. J.; Bertrand, E. M.; Alexander-Ozinskas, M.; Deng, D.; Moe, L. A.; van Beilen, J. B.; Danahy, M.; Groves, J. T.; Austin, R. N. Profiling mechanisms of alkane hydroxylase activity in vivo using the diagnostic substrate norcarane. *Chem. Biol.* **2007**, *14*, 165−172.
(46) Iliescu, A.; Oppenheim, J. J.; Sun, C.; Dinca, M. Conceptual and Practical Aspects of Metal-Organic Frameworks for Solid-Gas Reactions. *Chem. Rev.* **2023**, *123*, 6197−6232.
(47) Neugebauer, M. E.; Sumida, K. H.; Pelton, J. G.; McMurry, J. L.; Marchand, J. A.; Chang, M. C. Y. A family of radical halogenases for the engineering of amino-acid-based products. *Nat. Chem. Biol.* **2019**, *15* (10), 1009−1016.
(48) Roach, P. L.; Clifton, I. J.; Hensgens, C. M. H.; Shibata, N.; Schofield, C. J.; Hajdu, J.; Baldwin, J. E. Structure of isopenicillinN synthase complexed with substrate and the mechanism of penicillin formation. *Nature* **1997**, *387* (6635), 827−830.
(49) Ye, S.; Neese, F. Nonheme oxo-iron(IV) intermediates form an oxyl radical upon approaching the C-H bond activation transition state. *Proc. Natl. Acad. Sci. U.S.A.* **2011**, *108* (4), 1228−1233.
(50) Solomon, E. I.; Goudarzi, S.; Sutherlin, K. D. $O_2$ Activation by Non-Heme Iron Enzymes. *Biochemistry* **2016**, *55* (46), 6363−6374.
(51) Matthews, M. L.; Neumann, C. S.; Miles, L. A.; Grove, T. L.; Booker, S. J.; Krebs, C.; Walsh, C. T.; Bollinger, J. M., Jr Substrate positioning controls the partition between halogenation and hydroxylation in the aliphatic halogenase, SyrB2. *Proc. Natl. Acad. Sci. U.S.A.* **2009**, *106* (42), 17723−17728.
(52) Vennelakanti, V.; Mehmood, R.; Kulik, H. J. Are Vanadium Intermediates Suitable Mimics in Non-Heme Iron Enzymes? An Electronic Structure Analysis. *ACS Catal.* **2022**, *12* (9), 5489−5501.
(53) Que, L. J.; Puri, M. Toward the Synthesis of More Reactive S = 2 Non-Heme Oxoiron(IV) Complexes. *Acc. Chem. Res.* **2015**, *48*, 2443−2452.
(54) Galeotti, M.; Bietti, M.; Costas, M. Catalyst and Medium Control over Rebound Pathways in Manganese-Catalyzed Methylenic C-H Bond Oxidation. *J. Am. Chem. Soc.* **2024**, *146* (13), 8904−8914.
(55) Galeotti, M.; Vicens, L.; Salamone, M.; Costas, M.; Bietti, M. Resolving Oxygenation Pathways in Manganese-Catalyzed C(sp3)-H Functionalization via Radical and Cationic Intermediates. *J. Am. Chem. Soc.* **2022**, *144* (16), 7391−7401.


https://doi.org/10.1021/jacs.5c05557
J. Am. Chem. Soc. 2025, 147, 21325−21330